

# Nanoscale incipient asperity sliding and interface micro-slip assessed by the measurement of tangential contact stiffness

Y.F. Gao,<sup>a,b,\*</sup> B.N. Lucas,<sup>c</sup> J.C. Hay,<sup>c</sup> W.C. Oliver<sup>d</sup> and G.M. Pharr<sup>a,e</sup>

<sup>a</sup>Department of Materials Science and Engineering, University of Tennessee, Knoxville, TN 37996, United States

<sup>b</sup>Computer Science and Mathematics Division, Oak Ridge National Laboratory, Oak Ridge, TN 37831, United States

<sup>c</sup>Fast Forward Devices, LLC, Knoxville, TN 37931, United States

<sup>d</sup>Nano Instruments Innovation Center, MTS Systems Corporation, Oak Ridge, TN 37830, United States

<sup>e</sup>Metals and Ceramics Division, Oak Ridge National Laboratory, Oak Ridge, TN 37831, United States

Received 7 January 2006; revised 1 May 2006; accepted 5 May 2006

Available online 3 July 2006

Experiments with a multidimensional nano-contact system have shown that, prior to kinetic frictional sliding, there is a significant reduction of the tangential contact stiffness relative to the elastic prediction. The reduction occurs at contact sizes below about 50–200 nm for aluminum single crystals and several other materials. Using a cohesive interface model, we find that this reduction corresponds to a transition from a small-scale-slip to large-scale-slip condition of the interface.

© 2006 Acta Materialia Inc. Published by Elsevier Ltd. All rights reserved.

**Keywords:** Nanoindentation; Micromechanical model; Interface micro-slip

The development of the load and displacement sensing indentation techniques such as nanoindentation has led to a myriad of experimental and theoretical studies on small-scale mechanical behavior [1,2]. Typical indentation depths in such studies range from several nanometers to tens of micrometers. Sliding contact behavior in the same range of length scales, however, has received less attention because of the lack of quantitative measurement capabilities in the tangential direction. Although techniques such as the atomic force microscopy (AFM) [3] and the surface force apparatus (SFA) [4] can quantitatively measure the friction force and tangential contact stiffness, the range of measured contact stiffnesses is then either too small (less than about 100 N/m for AFM) or too large (greater than about 10<sup>6</sup> N/m for typical SFA). These limitations severely restrict the use of the AFM and SFA in the study of nano- and meso-scale mechanical properties during multiaxial contacts.

In order to bridge the gap between the length scales, a multidimensional nano-contact system [5] has been developed based on state-of-the-art nanoindentation technology. This instrument provides tremendous opportunities for the fundamental investigation of interface plasticity and mechanisms of friction and wear at small scales. The 3D system was produced by coupling three 1D nanoindentation actuators in orthogonal directions. Each axis of the system maintains the quantitative measurement capabilities (i.e. resolution, accuracy and reproducibility) of the 1D system with a range of measured normal/tangential contact stiffnesses between about 100 and 10<sup>6</sup> N/m. It is thus suitable for studying elastic and plastic deformation properties during nano- and micro-scale sliding contact. The unique aspect of the system is that the force along each axis can be independently controlled and the displacement along each axis of motion independently measured. Additional details of the experimental setup can be found in [5].

Figure 1 gives the measured contact stiffness along three directions against the penetration depth for a Berkovich diamond indenter driven into single-crystal aluminum. It should be pointed out that the multiaxial contact stiffnesses were measured by employing the continuous stiffness measurement technique in the three orthogonal directions [1,2,6]. This is a frequency-specific

\* Corresponding author. Address: Department of Materials Science and Engineering, University of Tennessee, Knoxville, TN 37996, United States. Tel.: +1 865 974 2350; fax: +1 865 974 4115; e-mail: [ygao7@utk.edu](mailto:ygao7@utk.edu)

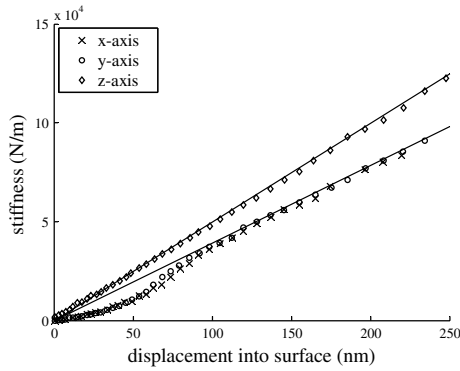


**Figure 1.** The measured contact stiffness in three dimensions plotted against the penetration depth of a Berkovich indenter into the surface of a bulk aluminum single crystal [5]. The two solid lines fit the elastic solutions. The transient region at small indentation depths (<100 nm for this material) is due to the interface slip (or called interface micro-slip).

testing method in which a small harmonic force is applied to the indenter and the harmonic response of the displacement and the phase angle shift are measured; the stiffness can be deduced by vibrational analysis. The harmonic force is controlled such that the amplitude of the resulting displacement oscillation is maintained at a constant value, that being 0.7 nm in the experiments presented in Figure 1. It is typically believed that, for such a small amplitude of displacement oscillation, the contact stiffness should be a constant value given by the elastic solution. The normal contact stiffness in Figure 1 is indeed linear with the contact penetration depth (that is, linear with the contact size for a Berkovich indenter); however, the tangential contact stiffness is only so when the penetration depth is larger than about 100 nm. Elastic contact mechanics predicts that the ratio of the tangential to normal contact stiffness is given by  $2(1-v)/(2-v)$ . A Poisson's ratio of  $0.346 \pm 0.017$  is deduced by fitting the data at large indentation depths (>100 nm). This paper is concerned with the transient region at small indentation depths. A micromechanical model is developed next to explain the significant reduction of the tangential contact stiffness at contact sizes of about 50–200 nm.

Consider an axisymmetric indenter sliding against a half-space as shown in Figure 2. The contact size is assumed to be determined solely by the normal load, since the applied tangential load is too small to cause the growth of the contact area during sliding. When adhesive forces play a significant role, this assumption still holds when the contact behavior approaches the Johnson–Kendall–Roberts limit [7]. Because the dissimilarity in the elastic constants of the two solids gives only a minor correction and the diamond indenter is much stiffer than the deforming material, we assume for simplicity that the two materials have the same elastic properties by using the composite moduli [6].

Assume that the two solids are bonded perfectly together, i.e., the two surfaces inside the contact zone have no relative tangential motion. The elastic solution [6] gives the traction distribution  $\sigma_{xz}^{\text{elastic}}(r)$  inside the contact zone and the tangential stiffness  $S_x^{\text{elastic}}$ :

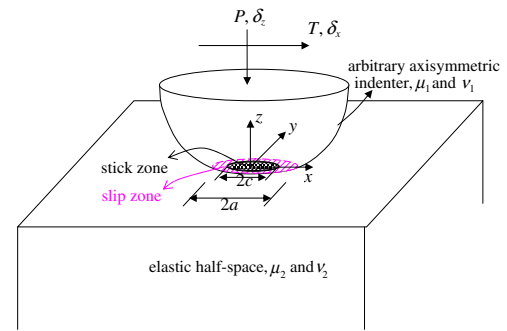


**Figure 2.** Schematic of incipient asperity sliding and the conventions used in its analysis. Because of the circumferential shear stress singularity predicted by the elastic solution, the two contacting surfaces slip against each other at the contact edge (i.e., causing a relative motion), and stick inside (i.e., undergoing the same tangential displacement).

$$\sigma_{xz}^{\text{elastic}} = \frac{T}{2\pi a \sqrt{a^2 - r^2}}, \quad S_x^{\text{elastic}} = \frac{dT}{d\delta_x} = 8a\mu^*, \quad (1)$$

where  $T$  and  $\delta_x$  are the tangential force and displacement (applied at distant reference points) respectively,  $a$  is the contact size,  $r = \sqrt{x^2 + y^2}$  is the radial coordinate, and the composite shear modulus is  $\mu^* = [(2 - \nu_1)/\mu_1 + (2 - \nu_2)/\mu_2]^{-1}$  with shear moduli  $\mu_1$  and  $\mu_2$  and Poisson's ratios  $\nu_1$  and  $\nu_2$  for the two contacting solids. Consequently, the tangential contact stiffness is directly proportional to the contact size and the composite shear modulus, and is independent of the tangential load and the tangential displacement. The normal contact stiffness is given by  $S_z^{\text{elastic}} = dP/d\delta_z = 2aE^*$ , where  $E^* = [(1 - \nu_1^2)/E_1 + (1 - \nu_2^2)/E_2]^{-1}$  with Young's moduli  $E_1$  and  $E_2$  for the two solids. For a rigid indenter, we get  $S_x^{\text{elastic}}/S_z^{\text{elastic}} = 2(1 - \nu)/(2 - \nu)$ , where  $\nu$  is Poisson's ratio of the deforming material. This is the theoretical foundation for the method used to obtain the Poisson's ratio in Figure 1.

As shown in Eq. (1), the interface shear stress field has an inverse-square-root singularity at the contact edge ( $r \rightarrow a^-$ ), which must be regularized, possibly by interface slip or shear-induced plastic deformation. The latter is usually difficult at small scales, so the focus here is on interface slip. For a slipping contact, the tangential shear stress at the contact edge may be limited by the Coulomb friction (i.e.,  $\sigma_{xz} \leq -q\sigma_{zz}$  with the friction coefficient  $q$ ), as described in the classic Cattaneo–Mindlin model [6]. However, Coulomb friction is a macroscopic phenomenon due to rough surface contacts; that is, it arises from a statistical average of multiple asperities in sliding contact [6,8]. The study presented in this paper is concerned with single-asperity frictional behavior, for which Coulomb friction does not formally apply. The micromechanical model we envision is similar to the Cattaneo–Mindlin model except that the mechanism of interface (micro-)slip is fundamentally different. We assume that the interface shear stress is limited by a shear strength  $\tau_0$ . This strength is similar to that used in the cohesive interface model for a mode II crack [9]. Stress-field solutions for the cohesive interface model are well documented for various crack shapes [10]. This model has also been used to explain

the coupling between adhesion and friction [11], but its utility in modeling the tangential contact stiffness has not been fully addressed before.

Referring again to Figure 2, the boundary value problem to be solved is an externally circular crack subjected to a faraway tangential force and crack interface shear traction,  $\sigma_{xz}(r) = \tau_0$ , at  $c \leq r \leq a$ . From [9–11], the interface shear stress distribution, the total applied force, and the tangential displacement at the reference point are given by

$$\sigma_{xz}(r) = \frac{\tau_0}{\pi} \cos^{-1} \left\{ \frac{2c^2 - a^2 - r^2}{a^2 - r^2} \right\}, \quad r \leq c, \quad (2)$$

$$T = 2\tau_0 a^2 \left[ \cos^{-1} \frac{c}{a} + \frac{c}{a} \sqrt{1 - \left(\frac{c}{a}\right)^2} \right], \quad (3)$$

$$\delta_x = \frac{\tau_0 a}{2\mu^*} \sqrt{1 - \left(\frac{c}{a}\right)^2}. \quad (4)$$

The tangential contact stiffness can be computed from Eqs. (3) and (4), namely,  $S_x = dT/d\delta_x = 8c\mu^*$ , which is proportional to the stick zone size  $c$ .

If  $2\mu^*\delta_x/a\tau_0$  is small (in comparison to unity), the tangential contact stiffness is indistinguishable from the elastic contact solution in Eq. (1), and the size of the stick zone approaches the contact size, i.e.,  $c/a \rightarrow 1^-$ . The interface is then characterized by the small-scale-slip (SSS) condition. On the other hand, for a large  $2\mu^*\delta_x/a\tau_0$ , even an infinitesimally small tangential load can cause a large slip zone size ( $c \ll a$ ), and the tangential contact stiffness can be significantly lower than the elastic solution. The interface is then in the large-scale-slip (LSS) condition. When  $c/a = 0$ , the whole interface slips and the sliding is controlled by kinetic friction. The maximum shear force prior to the kinetic friction is  $T_{\text{kinetic}} = \pi\tau_0 a^2$ , and the corresponding tangential displacement is  $\delta_{x,\text{kinetic}} = a\tau_0/2\mu^*$ .

The contact stiffness in Figure 1 is measured by the continuous stiffness measurement method, in which an oscillation between 0 and  $\delta_{\text{max}}$  is prescribed for the tangential displacement. Defining  $a_{\text{crt}} = 2\mu^*\delta_{\text{max}}/\tau_0$  and  $S_{x,\text{crt}} = 8a_{\text{crt}}\mu^*$ , the stiffness can be written as

$$\frac{S_x}{S_{x,\text{crt}}} = \begin{cases} \frac{a}{a_{\text{crt}}} \sqrt{1 - \left(\frac{a_{\text{crt}}\delta_x}{a\delta_{\text{max}}}\right)^2}, & \frac{a\delta_{\text{max}}}{a_{\text{crt}}\delta_x} \geq 1, \\ 0, & \frac{a\delta_{\text{max}}}{a_{\text{crt}}\delta_x} < 1. \end{cases} \quad (5)$$

In order to describe the stiffness measured by the continuous stiffness measurement method [1,2], we approximate it by a weighted average over  $\delta_x \in [0, \delta_{\text{max}}]$ , namely,

$$\bar{S}_x = \frac{1}{\delta_{\text{max}}} \int_0^{\delta_{\text{max}}} w S_x d\delta_x, \quad (6)$$

where the weight function can be chosen as  $w = 1$  (uniform weighted average) or  $w = \frac{\pi}{2} \sin\left(\frac{\pi\delta_x}{2\delta_{\text{max}}}\right)$  (biased weighted average).

The transient region in Figure 1 can now be quantitatively described as the transition from the SSS condition to the LSS condition. When the contact size is below  $a_{\text{crt}}$ , even a small displacement oscillation  $\delta_{\text{max}}$ , relative

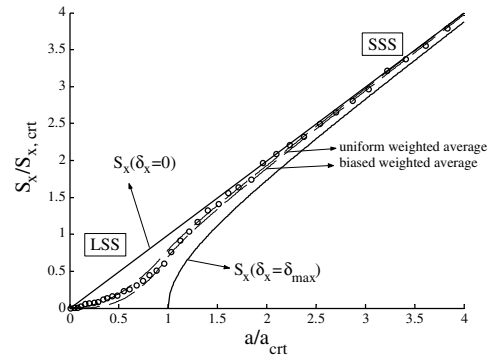


**Figure 3.** The tangential contact stiffness (normalized by  $S_{x,\text{crt}} = 8a_{\text{crt}}\mu^*$ ) plotted against the contact size (normalized by  $a_{\text{crt}} = 2\mu^*\delta_{\text{max}}/\tau_0$ ). The two types of weighted-average values are defined in Eq. (6). Curve fitting gives  $a_{\text{crt}} = 192$  nm using the data in Figure 1 (circles, aluminum single-crystal). Small-scale slip (SSS) occurs for large contact sizes, while large-scale-slip (LSS) is the opposite.

to the contact size, is large enough to give rise to LSS in the interface, and the tangential contact stiffness becomes much smaller than that predicted by the elastic no-slip solution. Figure 3 plots the measured tangential contact stiffness (data marked by circles in Figure 1 for single-crystal aluminum) and the predictions of Eqs. (5) and (6) against the contact size. The composite shear modulus  $\mu^*$  and Poisson’s ratio  $\nu$  can be obtained from the elastic sliding contact in the large indentation-depth range in Figure 1. Consequently, the only adjustable parameter in fitting the measured data in the small indentation-depth range in Figure 1 is  $a_{\text{crt}}$ . Since the weighted average in Eq. (6) is only an approximation of the continuous stiffness measurement technique, the critical contact size is fitted so that the circles in Figure 3 are bounded by the two dashed curves. For single-crystal aluminum studied in Figure 3, we obtain  $a_{\text{crt}} = 192$  nm,  $\tau_0 = 116$  MPa, and  $\mu^*/\tau_0 = 137$ . For fused silica,  $\nu = 0.17$ ,  $a_{\text{crt}} = 104$  nm,  $\tau_0 = 226$  MPa, and  $\mu^*/\tau_0 = 74.2$ . For polycrystalline gold,  $\nu = 0.42$ ,  $a_{\text{crt}} = 103$  nm,  $\tau_0 = 187$  MPa, and  $\mu^*/\tau_0 = 73.5$ .

To this point, the interface slip phenomenon has been assumed to be governed by the interface shear strength  $\tau_0$ . Based on a recent dislocation plasticity model [12,13], a possible physical origin for this rather phenomenological parameter is now presented. Because the contact size is in the range of 10–1000 nm, the interface slip and the sliding-contact strength are determined by the collective behavior of dislocations at the mesoscopic length scale. This being the case, the interface shear strength would be size-dependent. A dislocation can be nucleated from the contact edge if the stress intensity factor reaches a critical value,  $K_{\text{crt}} = \sqrt{\mu\gamma_{\text{us}}/(1-\nu)}$ , where  $\gamma_{\text{us}}$  is the unstable stacking energy, a material parameter [14]. Elastic solution in Eq. (1) gives the stress intensity factor  $K_{\text{II}} = T \cos\theta/2a\sqrt{\pi a}$  and  $K_{\text{III}} = T \sin\theta/2a\sqrt{\pi a}$  at the contact edge where  $\theta = \tan^{-1}(y/x)$ , implying that the interface shear strength  $\tau_0$  is proportional to  $1/\sqrt{a}$ . The size of the dislocation nucleation process zone can be estimated as  $\mu b^2/8\gamma_{\text{us}}$  [14,15], so that dislocation nucleation cannot occur when the contact size is less than this critical value

(on the order of several to ten nanometers). Consequently, the upper bound of  $\tau_0$  is the theoretical shear strength (about one tenth of the shear modulus). On the other hand, for large contact sizes, it is anticipated that the incipient asperity sliding is accommodated by gliding multiple dislocations. The classic analysis of dislocation pileup against an obstacle (a grain boundary, for example) shows that the number of dislocations is  $N_{\text{disl}} \approx \tau_0 a(1 - \nu)/\mu b$  for an applied shear stress  $\tau_0$  [16]. A scaling relation of  $\tau_0 \propto 1/\sqrt{a}$  clearly indicates that the number of dislocations will increase with increasing contact size. Thus, the lower bound of  $\tau_0$  is the lattice resistance stress (often called the Peierls stress) of the interface.

The size-dependence of  $\tau_0$  indicates that its measurement by AFM [3] should approach the theoretical strength (i.e.,  $\mu^*/\tau_0 \approx 10$ ) while that by SFA [4] would be the effective Peierls stress (i.e.,  $\mu^*/\tau_0 \approx 1000$ ). Our experiments give  $\mu^*/\tau_0 \approx 100$ . However, considering two other points, the fitted values of  $\tau_0$  in Figure 3 should be viewed as only qualitative in nature. First, the above size-dependence of  $\tau_0$  is predicted to occur at a length scale  $a \approx 1000b$  (assuming a pileup of 10 dislocations), roughly on the same order of magnitude as the critical contact size for the transition from SSS to LSS. Second, in our experimental work to date, the measured tangential contact stiffness has been an average quantity derived from the continuous stiffness measurement technique, which averages over a large variation of the slip-zone size. If the relation between  $a_{\text{crt}}$  and  $\delta_{\text{max}}$  is found to be nonlinear ( $\delta_{\text{max}}$  can be easily varied in the continuous stiffness measurement method), it is anticipated that one can quantify the size-dependence of  $\tau_0$ . This is amenable to experimental study and verification.

The micromechanical model presented above is essentially a way of regularizing the stress singularity at the contact edge. The validity of assumptions in this model is discussed below. First, solutions in Eqs. (1)–(4) are valid regardless of the indenter shape, as long as the indenter is smooth and axisymmetric [6]. Second, surface roughness may significantly change the contact pressure distribution, but will not change the contact stiffness noticeably since the root-mean-square roughness (less than a few nanometers for our samples) is much less than the indentation depth [8,17]. Third, the tangential contact stiffness can be fitted nicely by the elastic Mindlin solution in (1) at large indentation depths, which indicates that the tangential load (corresponding to a tangential displacement of 0.7 nm) is very small and cannot cause any noticeable plastic deforma-

tion. The normal contact, whether being elastic or elastic–plastic, will not affect the solutions in the tangential direction given earlier.

In summary, this paper gives a theoretical analysis for nanoscale incipient asperity sliding, especially for the dependence of the tangential contact behavior on the contact size. Comparing a cohesive interface model to experiments performed using a multidimensional nanocontact system, the significant reduction of the measured tangential contact stiffness, relative to the elastic prediction, is found to correspond to a transition from small-scale-slip (SSS) to large-scale-slip (LSS) condition of the interface.

This work was supported in part by the University of Tennessee and the Tennessee Advanced Materials Laboratory. Research at the Oak Ridge National Laboratory was sponsored by the Division of Materials Science and Engineering, Office of Basic Energy Science, US Department of Energy, under contract DE-AC05-00OR22725 with UT-Battelle, LLC.

- [1] W.C. Oliver, G.M. Pharr, *J. Mater. Res.* 7 (1992) 1564.
- [2] W.C. Oliver, G.M. Pharr, *J. Mater. Res.* 19 (2004) 3.
- [3] R.W. Carpick, N. Agrait, D.F. Ogletree, M. Salmeron, *Langmuir* 12 (1996) 3334.
- [4] A.M. Homola, J.N. Israelachvili, P.M. McGuiggan, J.W. Hellgetch, *Wear* 136 (1990) 65.
- [5] B.N. Lucas, J.C. Hay, W.C. Oliver, *J. Mater. Res.* 19 (2004) 58.
- [6] K.L. Johnson, *Contact Mechanics*, Cambridge University Press, Cambridge, 1985.
- [7] K.L. Johnson, K. Kendall, A.D. Roberts, *Proc. R. Soc. London* 324A (1971) 301.
- [8] Y.F. Gao, A.F. Bower, *Proc. R. Soc.* 462A (2006) 319.
- [9] B.A. Bilby, A.H. Cottrell, K.H. Swinden, *Proc. R. Soc. London* 272A (1963) 304.
- [10] H. Tada, P.C. Paris, G.R. Irwin, *The Stress Analysis of Cracks Handbook*, third ed., ASME, New York, 2000.
- [11] K.L. Johnson, *Proc. R. Soc. London* 453A (1997) 163.
- [12] J.A. Hurtado, K.-S. Kim, *Proc. R. Soc. London* 455A (1999) 3363.
- [13] J.A. Hurtado, K.-S. Kim, *Proc. R. Soc. London* 455A (1999) 3385.
- [14] J.R. Rice, *J. Mech. Phys. Solids* 40 (1992) 239.
- [15] Y.F. Gao, A.F. Bower, *Modell. Simulat. Mater. Sci. Eng.* 12 (2004) 453.
- [16] J.D. Eshelby, W.T. Read, W. Shockley, *Acta Metall.* 1 (1953) 251.
- [17] E. Ciavarella, G. Murolo, G. Demelio, J.R. Barber, *J. Mech. Phys. Solids* 52 (2004) 1247.